HHS Public Access

Author manuscript

ACS Appl Mater Interfaces. Author manuscript; available in PMC 2018 September 13.

Published in final edited form as:

ACS Appl Mater Interfaces. 2017 September 13; 9(36): 30318–30328. doi:10.1021/acsami.7b06742.

3D-Printed pHEMA Materials for Topographical and Biochemical Modulation of Dorsal Root Ganglion Cell Response

Adina Badea[a], **Joselle M. McCracken**[a], **Emily G. Tillmaand**[c], **Mikhail E. Kandel**[d], **Aaron W. Oraham**[a], **Molly B. Mevis**[a], **Stanislav S. Rubakhin**[a], **Gabriel Popescu**[d], **Jonathan V. Sweedler**[a,c,*], and **Ralph G. Nuzzo**[a,b,*]

[a]School of Chemical Sciences, University of Illinois-Urbana Champaign, Urbana, IL 61801, United States of America

[b]School of Chemical Science and Engineering, KTH Royal Institute of Technology, Stockholm, Sweden

[c]Neuroscience Program, University of Illinois-Urbana Champaign, Urbana, IL 61801, United States of America

[d]Department of Electrical and Computer Engineering, University of Illinois-Urbana Champaign, Urbana, IL 61801, United States of America

Abstract

Understanding and controlling the interactions occurring between cells and engineered materials are central challenges towards progress in the development of biomedical devices. In this work, we describe materials for direct ink writing (DIW), an extrusion-based type of 3D printing, that embed a custom synthetic protein (RGD-PDL) within the microfilaments of 3D-hydrogel scaffolds to modify these interactions and differentially direct tissue-level organization of complex cell populations *in vitro*. The RGD-PDL is synthesized by modifying poly-D-lysine (PDL) to varying extents with peptides containing the integrin-binding motif Arg-Gly-Asp (RGD). Compositional gradients of the RGD-PDL presented by both patterned and thin-film poly-(2-hydroxyethyl) methacrylate (pHEMA) substrates allow the patterning of cell-growth compliance in a grayscale form. The surface chemistry-dependent guidance of cell growth on the RGD-PDL-modified pHEMA materials is demonstrated using a model NIH-3T3 fibroblast cell line. The formation of a more complex cellular system — organotypic primary murine dorsal root ganglion (DRG) – in culture is also achieved on these scaffolds, where distinctive forms of cell growth and migration guidance are seen depending on their RGD-PDL content and topography. This experimental platform for the study of physicochemical factors on the formation and the reorganization of

*Corresponding Authors: r-nuzzo@illinois.edu, jsweedle@illinois.edu.

Supporting Information

Supplemental methods; CFM images showing control experiments for the biocompatibility assessment of RGD-modified PDL surface treatments; CFM images showing complete experiment series showing fibroblast response to RGD-PDL surface treatments; Phase contrast micrographs of DRG cells cultured on surfaces treated with RGD-modified PDL; Time-lapse phase contrast micrographs of DRG cells on RGD-modified PDL-treated surfaces; CFM images of DRG cell networks; Scheme of the glia-neurons association quantification algorithm; Signal intensity profiles and quantification of glia-neurons association; Phase contrast micrographs of DRG cell culture on 3D DIW structures; Phase contrast micrographs illustrating the impact of aspect ratios and diffusible molecules on cell outgrowth; DRG cell growth on 3D scaffolds;

organotypic cultures offers useful capabilities for studies in tissue engineering, regenerative medicine, and diagnostics.

Graphical Abstract

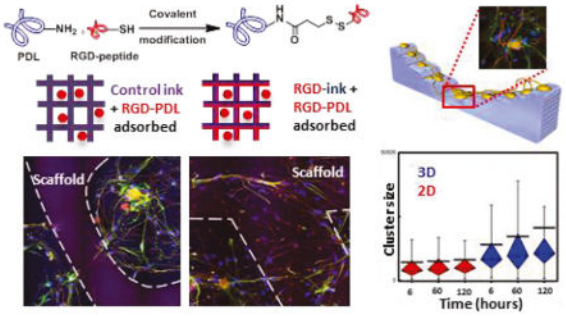

Keywords

4D Printing; Biologically compliant materials; Programmable cell-scaffold interactions; 3D cell culture; Functional soft materials; Dorsal root ganglion (DRG); Gels

1. Introduction

The ability to reconstruct and manipulate neuronal networks *in vitro* has important applications across a number of fundamental and applied research fields that include elucidating the mechanisms behind neuronal interactions,[1–5] nerve damage and repair[6–9] as well as haptic interfacing to prosthetic devices.[10,11] Programming the spatial arrangement of neuronal circuits *ex vivo* has been widely explored via a variety of approaches including chemically and topographically guided neuronal process outgrowth and interconnection (e.g. within microchannel architectures[12–15] or via chemical/textural features established by micropatterning[16–19]). These approaches have especially benefitted from advances made in soft lithography,[20,21] particularly in microcontact printing (μCP)[22–26] and stenciling.[7,27–29] A need and opportunity remains, however, to answer fundamental biological questions that might aid the discovery of improved methods to replace or repair human neural tissues[30]—a factor motivating the study of 3D organotypic cultures that better mimic the complexities of *in vivo* systems than do 2D cultures or those using immortalized cell lines or homogenous cell populations.

Located proximally to the spinal cord, dorsal root ganglia (DRG) provide an important model for investigating the mechanisms of peripheral nervous system (PNS) injury and repair.[31] The DRG is a compact structure comprising cell bodies of primary sensory neurons, their processes, satellite and Schwann cells, as well as a variety of cells related to the immune and circulatory systems.[32,33] The involvement of DRG sensory neurons in a large number of frequently occurring pathological conditions including injury-associated neuropathic pain,[34] and the ability of these cells to develop functional networks and even form organotypic structures *in vitro,*[35] make them a good model for the evaluation of new

biocompatible materials and engineered microdevices designed to promote the repair of human neural structures—interests motivating this study.

The scaffolds materials developed to-date for primary DRG cell culture remain limited as to the degree of control they can provide over tissue-level organization (as are required for viable clinical approaches to tissue regeneration or repair).[36–43] Improvements will likely require significant advances made in both the development of new materials and means of 3D fabrication to provide scaffolds that can better promote/sustain the necessary forms of cell growth and integration. Here we examine methods that have the capacity to more controllably direct cellular development in tissue cultures *in vitro*, by exploiting direct ink writing (DIW) and new inks for programmable chemical patterning of hydrogel-based microscaffolds. We describe capabilities that complement other scaffold fabrication methods (including inkjet,[44–47] microextrusion,[48–50] and laser-assisted fabrication[51–53]) while exploiting the unique capacity of DIW to pattern soft materials with tunable physicochemical/mechanical properties.[54–59]

We use an exemplary hydrogel material amenable to 3D printing by DIW, the neutral hydrophilic polymer poly(2-hydroxyethyl) methacrylate (pHEMA) that has been widely used in the manufacturing of contact and intraocular lenses, as well as coatings of stents.[60,61] Unmodified pHEMA acts as a ‘blank canvas’—a bioinert material that effectively resists cellular attachment and growth[62,63]. Chemical modifications of pHEMA, however, can promote cell attachment and development in culture.[63] In previous work, we modified the compositional attributes of pHEMA hydrogels (pHH) to tune their gel mesh properties, mechanics, and their subsequent equilibrium absorption of poly-L-lysine (PLL). We have shown these physicochemical features to broadly impact the cell growth compliance of both pHH films and 3D microscaffolds in NIH/3T3 murine fibroblast and MC3T3-E1 cell cultures.[64] When modified with poly-D-lysine (PDL), these microperiodic scaffolds also allow the development and guidance of networks of rat primary hippocampal neurons.[65]

Here we use DIW and newly designed materials to fabricate multifunctional hydrogel microscaffolds that are able to exert better control on cell growth, attachment and migration. The system builds upon the geometric and compositional cues present within pHH-based hydrogel patterns and microscaffolds and focuses on modulating cell-scaffold interactions via integrin signaling. Using hydrogel interfaces modified by the integrin recognition domain-mimetic [66,67] RGD-PDL absorbed within the gel matrix, we first demonstrate the universality of this approach using a model cell line, NIH/3T3 murine fibroblasts, and then advance to comprehensively directing primary DRG cell populations. The responses of the isolated DRG cells to the compositional features of the substrates are assessed in 2D cell cultures and on topographically more complex 3D scaffolds. The RGD-PDL-modified gel materials allow direct cellular network and organotypic structure formation without need for pre-seeding the devices with Schwann cells as is typical for DRG cultures carried out in engineered devices.[38,42,43] The insights developed in this study suggest materials-directed strategies and fundamental design rules that can yield access to a gradient of *in vitro* growth compliance with a variety of cells.

2. Experimental Section

Unless otherwise noted, all starting materials, solvents, and reagents were acquired from commercial suppliers and used without further purification. The list of all reagents and the composition of all media used for cell culture are listed in the Supporting Information, Supplemental Methods.

Chemical Modification of PDL with RGD-containing Peptides

A 2 mg/mL solution of PDL (30–70 kDa) in HEPES buffer was reacted with 10, 25, 50, and 100 μM solutions of N-Succinimidyl 3-[2-pyridyldithio]-propionate (SPDP) in DMSO for 30 mins at room temperature (RT). The reaction mixtures were filtered through spin desalting columns, then subjected to 10, 25, 50, and 100 μM solutions of either Ac - GCGYGRGDSPG - NH_2 or *cyc*(RGDyC) and stirred at 4°C overnight. The products were purified by filtration through spin desalting columns and analyzed by UV-Vis. Details regarding the quantification of the degree of modification are given in the Supplemental Methods.

Micropattern and 3D Scaffold Fabrication

Glass substrates (12 mm diameter, 0.17 mm thickness, Warner Instruments) are cleaned and soaked in a 5% 3-(Trimethoxysilyl)propyl methacrylate (Sigma) in toluene solution at 60°C overnight and rinsed with isopropanol. pHH micropatterns and 3D scaffolds are fabricated using an AGS-1000 high precision custom gantry with an A3200 integrated automated motion system (Aerotech). Complete protocols are given in Supplemental Methods.

NIH/3T3 Fibroblasts Seeding and Culture

The initial cell stock (density of ~1×10^6 cells/ml) is transferred to a T-75 cell culture flask and maintained in 9 mL of complete media containing DMEM, that consists of 4.5 g/L glucose, 4 mM glucose, 1mM sodium pyruvate, 1.5 g/L sodium bicarbonate, supplemented with 10% calf bovine serum and 1% Penicillin/Streptomycin. The cells are maintained according to standard protocols, detailed further in the Supplemental Methods.

Primary Adult Rat DRG Dissociation and Seeding

Approximately 20 lumbar and thoracic DRGs from an adult rat were collected and stored in Hibernate A up to 2 days before seeding (the protocol for adult rat DRG isolation is detailed in Supplemental Mehtods). The Hibernate media was then removed. The DRGs were treated with 0.25% collagenase in DRG physiological media for 1.5 h at 37°C, shaken a few times during incubation and strongly upon completion of the incubation period. The DRGs were centrifuged (200 *x* g) for 2–3 min to remove supernatant, and washed with HBSS. After another centrifugation, the HBSS was mostly removed and the DRG were incubated in 0.25% trypsin with EDTA for 15 mins at 37°C. The DRGs were centrifuged to remove supernatant, re-suspended in DRG media + 1% FBS for 50 s to inactivate trypsin, and triturated. After 2 min, once some of the pellet re-settled, the supernatant was collected and centrifuged for 5 min at 200 *x* g. The resulting pellet was washed with HBSS and centrifuged to remove supernatant. Pelleted cells were re-suspended in the desired amount of DRG media containing the glial inhibitor AraC, usually 1 mL per 10 original DRGs. After

cell seeding, the scaffolds were incubated for 10 min at 37°C to allow for cell attachment before an additional 2 mL per Petri dish (3 mm in diameter) of DRG media is added. The media is changed every 7 days. The concentration of AraC in the DRG media is kept at 0.3 μM from the moment of cell seeding until the end of the culture.

Cellular Fixation and Imaging

All light microscopy studies of the NIH/3T3 embryonic murine fibroblasts were performed on a Zeiss (Thornwood, NY) Axiovert 40 CFL inverted microscope. All light microscopy imaging of the primary adult rat dorsal root ganglia cells was performed on Zeiss Axiovert 25 inverted microscope, with a phase contrast filter (Ph 1-0,4). Confocal images were acquired using a Zeiss LSM7 Live Confocal Fluorescence Microscope. Fiji image analysis software with the MTrackJ plug-in was used for the cell tracking and other types of analysis. Complete details regarding fixation protocols, imaging parameters, and analysis protocols are given in the Supplemental Methods.

Long Term Imaging with SLIM

Quantitative phase imaging[68] was performed using a Zeiss Z1 microscope coupled to a SLIM module (CellVista SLIM Pro, PhiOptics Inc.). SLIM augments an existing phase contrast microscope by providing quantitative optical pathlength information associated with the specimen of interest.[69] Because it is a label-free modality, SLIM is suitable for long term imaging, without the limitations associated with photobleaching and phototoxicity. To study the growth and proliferation of DRG cells on 3D scaffolds, we monitored two volumes of (17.5 mm) × (17.5 mm) × (0.5 mm) over a period of 128.5 hours with a 10x/0.3 objective. The resulting 19TB of data were assembled offline, using a Python software module developed in-house. More details on image analysis are given in the Supplemental Methods.

Statistical analysis

The values of the NIH/3T3 Fibroblast cell densities and DRG cell coverage fractions are expressed in the form Mean ± Standard Deviation (SD). Eleven rats were used in the experiments, with minimum three biological repeats for each studied condition. Using OriginPro version 8.6 (OriginLab Corp., Northampton, MA, USA), an analysis of variance (ANOVA) was performed. When appropriate main effects were detected, Tukey's post-hoc (for unequal n) tests were used to make pair-wise comparisons (α set to $p < 0.05$). The Tukey mean comparison tables are given in the Supporting Information file.

3. Results and Discussion

3.1 Chemical Modifications of Poly-D-Lysine by RGD Peptides and Optimization for pHH Supported Cultures Using NIH/3T3 Cells

The most common protein treatments used to modify a hydrogel system such as pHH to allow cell attachment and growth are either extracellular matrix (ECM) proteins (such as fibronectin, vitronectin, and laminin) or a form of poly-lysine (PDL or PLL).[64,65] Many ECM proteins contain the arginine-glycine-aspartic acid (RGD) amino acid sequence as their cell attachment site.[66] The RGD sites of these adhesive proteins are recognized by a family of cell membrane receptors called integrins.[67] In contrast, poly-lysine increases

cellular attachment to surfaces through non-specific electrostatic interactions.[70,71] The strong, multi-segmental hydrogen-bonding interactions between poly-lysine and pHH gels lead to a marked (and generally irreversible) uptake of the protein by the polymeric scaffolds, which provides enhanced surface/interfacial interactions with cells. To mimic both of these recognition elements within a pHH scaffold and to reduce surface interactions with other ECM proteins, a chemically-modified PDL protein was synthesized. This was performed by covalently attaching cyclic or linear variants of RGD-containing peptides to PDL proteins via the heterobifunctional crosslinker N-Succinimidyl 3-[2-pyridyldithio]-propionate (SPDP, Fig. 1a and Supporting Information, Supplemental Methods, Figures S1 and S2). The efficacy of the coupling reaction was quantified spectrophotometrically via the release of the pyridine-2-thione coproduct, which absorbs strongly at 343 nm (Supplemental Methods).[72] The covalent attachment of the RGD-peptides to the PDL through this coupling reaction, as opposed to nonspecific adsorption/agglomeration, was confirmed by UV-Vis (Supplemental Methods, Figure S2) The stochastic nature of the PDL RGD-modification leads to the synthesis of PDL molecules with incomplete occupation of all reactive sites. This affords one level of control over the spatial presentation of the RGD motif within a modified pHEMA gel (see below).

The areal density of the RGD moiety is known to affect cellular responses in culture.[73] To determine the type and optimal degree of the RGD modification needed for DRG cellular cultures, a series of cyclic and linear RGD-PDL proteins (*cyc*(*lin*)RGD-PDL-1 through *cyc*(*lin*)RGD-PDL-4) was synthesized (Supplemental Methods). The extent of the modification for each type of RGD-PDL was quantified using a Trypan blue assay, which allowed the determination of the PDL concentration, as correlated with RGD-peptide stoichiometric data obtained via the specific absorbance of the pyridine-2-thione coproduct (Supplemental Methods).[74] All of the reaction conditions used in the series were selected to yield relatively small quantities of RGD peptide attached per PDL molecule (Table 1), not exceeding a 13.9:1 ratio of the recognition sequence to the much larger PDL macromolecule (Fig. 1b, Table 1, and Supplemental Methods). This corresponds to a modification of up to 4.1% of the total lysine amine moieties.

To survey the activities of the varying *cyc*(*lin*)RGD-PDL modifications towards promoting cellular attachment and growth-compliance, cultures made of a fast-growing cell line, NIH-3T3 murine fibroblasts, were are used as a model. The cells here were seeded at equal densities and grown for 24 h on pHH thin films that had been treated with PDL (type 0) or with one of either *cyc*RGD-PDL or *lin*RGD-PDL (types 1–4). The cell cultures that developed on the substrates were fixed and fluorescently stained with the nuclear stain DAPI and the F-actin stain rhodamine-phalloidin to quantitatively assess their morphological parameters (Figure 1c), including cellular spatial distribution. These data, summarized in Table 1, show that a type 1 PDL modification (made with either *cyc*RGD-PDL or *lin*RGD-PDL) yields cellular attachment/growth behaviors comparable to treatments made with unmodified PDL. In these three cases, cells aggregated in clusters with F-actin stain compacted around nuclei (Fig. 1d–1 and Fig. S3). We attribute the cluster formation in these systems to lower cellular adhesion to the pHH comparatively to intercellular adhesion.

In contrast, treatments with type 2 *cyc*RGD-PDL and *lin*RGD-PDL fostered fibroblast attachment/growth resulting in a uniform monolayered spatial cell distribution (Fig. 1d–2). Of these, *lin*RGD-PDL-2 showed a much higher attachment/growth propensity relative to *cyc*RGD-PDL-2 (Tukey's range test, $p < 0.006$, Table S1). Interestingly, this trend is reversed for the case of RGD-PDL type 3 (Fig. 1d–3). Here, the *cyc*RGD-PDL modification showed the highest fibroblast density within the tested *cyc*RGD-PDL series (Tukey's range test, $p < 0.0001$, Table S1), while the *lin*RGD-PDL-3 variant yielded a significantly lower cell density than *lin*RGD-PDL-2. The decline in fibroblast attachment/growth was much more pronounced for the RGD-PDL-4 treated pHH films (data not shown), yielding low fibroblast densities associated with the reduced affinity for cell attachment. The cells that did survive in this case were easily detached when exposed to mechanical forces during the fixation procedure (fluorescence imaging data could not be obtained for this experimental series). Fluorescence imaging data (including a positive control on a PDL-treated glass substrate) strongly demonstrates the differing impacts of the specific RGD-PDL protein treatments on growth compliance (Figures S3 and S4). The trends observed for the *cyc*(*lin*)RGD-PDL proteins reveal that pronounced differences in fibroblast attachment/growth and cell culture morphologies can be induced on pHH substrates modified via the absorptive uptake of RGD-PDL molecules possessing different integrin-binding peptide ratios. The *lin*RGD-PDL 2 protein demonstrated best performance in terms of the biocompatibility engendered for the fibroblast cell line. This approach can be used universally, to find the best type of RGD-PDL to modulate scaffold-cell interfaces for other cell lines/types.

3.2 Optimization of RGD-PDL Modifications of pHH Substrates for DRG Cell Growth Compliance

Following the initial screen of growth compliance described above, the development of organotypic DRG cell cultures on RGD-PDL-modified pHH thin films was also studied. Primary adult rat lumbar and thoracic DRGs were dissociated and heterogeneous suspensions of the cells seeded on thin-film gel substrates that had been treated as above, specifically with either PDL (type 0) or the type 1–4 modifications by either *cyc*RGD-PDL or *lin*RGD-PDL. A PDL-treated glass sample was used as a positive control. Once seeded onto their substrates, the DRG cells were exposed to a low concentration of cytosine arabinoside (AraC), an inhibitor of glial cell proliferation that helps maintain a stable population of the cultured primary cells over long culture intervals.[75]

Evaluation of the differences of growth compliance within the RGD-PDL modification series required a modified set of statistical parameters than were used to describe the fibroblast cultures. To account for the morphologies typical for cultured DRG cell populations, such as the clustering of cell bodies and the generation of elongated bundles of terminals, surface area fractions covered by both types of these cellular structures were quantitatively measured within randomly chosen sample areas. In these cultures, high surface area coverage is generally found to be associated with robust development of cell terminals including axons.

The data, given in Table 2 and shown in Figure 2a, demonstrate specific correlations of behaviors for the DRG cell cultures that are qualitatively similar to those seen in the 3T3 fibroblast growth series. In terms of the surface coverage of cellular structures, the *cyc*RGD-PDL-3 modified pHH films were found to elicit the best growth compliance (with ~43% of the surface covered at day 9).

This coverage is significantly higher than is observed in control experiments (Tukey's range test, $p < 0.0001$, Table S2).

Surface coverage fractions measured for the PDL control and each RGD-PDL treatment type are given graphically in Figure 2b. While the general trends seen in the DRG cell and fibroblast cell culture data sets are similar, the former developed best on pHH substrates modified by *cyc*RGD-PDL-3 (Fig. 2b, Figures S5 and S6). It is notable that, in the case of the DRG cell culture, the high modification levels present in the *cyc*(*lin*)RGD-PDL-4 systems do not potentiate cellular network development as well as the *cyc*RGD-PDL-3 variant does. They do, however, encourage some increase in cell culture surface coverage comparatively to *cyc*(*lin*)RGD-PDL modifications types 1 and 2. Taken together, these experiments show that DRG cell cultures grow and develop preferentially on a specific modified form of the pHH hydrogels (*cyc*RGD-PDL-3). In consequence of these results, we focused subsequent investigations on textural guidance in DRG cultures (see below) on *cyc*RGD-PDL-3 (referred to here after as **RGD-PDL**) modified materials.

3.3 Time-Lapse Microscopy and Immunohistochemical Analysis of DRG Cell Culture Architecture and Dynamics

A notable characteristic of DRG cell culture is its tendency to form multicellular organotypic structures as a result of increasingly organized cellular and structural migration over time. To provide a benchmark for the comparative analysis of different culturing conditions, including the 3D scaffolds examined below, these reorganizations were investigated using time-lapse microscopy of cell culture developed on pHH thin films that had been treated with RGD-PDL (Fig. 2c). The data demonstrates that the initial (<4 d in culture) random distribution of attached glial and neuronal cells begins to exhibit some structuring as a consequence of both anisotropic cell migration and terminal elongation (~10 d in culture). By 14 d in culture, cells that are morphologically consistent with neurons cluster together, forming ganglion-like structures. The exterior of these structures is occupied by glia-like cells exhibiting thin cell bodies. Individual or bundled cellular terminals are seen interconnecting the ganglion-like structures, exhibiting morphologies typical for functional neuronal networks. The terminals are often lined by cells that morphologically resemble Schwann cells. These observations indicate a cell distribution in culture similar to that in the native DRGs and nerves (vide infra). A representative set of time-lapse images for each *cyc*(*lin*)RGD-PDL treatment type is given as Figures S7–S12.

To determine the localization of the different cell types present in these complex cultures, we performed immunohistochemical staining and confocal fluorescent microscopy (CFM) analyses. Neurite-specific microtubule-associated protein 2 (MAP2) and glia-specific glial fibrillary acidic protein (GFAP) antibodies along with the nuclear stain DAPI were used to locate individual cells and distinguish neurons from glia in the culture. Cellular networks

formed on day 14 demonstrate a complex organization where widespread nuclei frequently co-localize spatially with both cellular terminals exhibiting MAP2 (red) and those exhibiting GFAP (green) immunostaining (Figure 2d). This observation indicates that glia-like cells form a bed for neuron outgrowth. Our data are in good agreement with information reported in literature for other DRG cell cultures.[76] Immunostaining of DRG cell clusters additionally indicates the coverage of large MAP2-expressing neuronal cell bodies by small GFAP-expressing satellite cells.

Close association between neuronal and glial cell terminals occurred extensively in the developing cultures. Neuronal processes, rich in microtubules, and GFAP-expressing cell terminals form complex networks. To analyze this interaction, we introduced an algorithm for quantification that focuses on specific fluorescence signals (red for MAP2 and green for GFAP) and measures the distances between the cellular sources for that signal using the closest nucleus as a reference point (Figure S14). Grayscale maps reflecting the degree of signal overlap were generated to help identify this interaction in cases of high and low association between the fluorescence signals corresponding to the two channels and the reference nucleus (Figure S14). The quantitative data obtained revealed predominant localization of the terminals of the two intertwining networks within 1 μm of each other (Figure S15). This observation suggests that some of the investigated neurites are myelinated by Schwann cells.[77] Additional images that show this characteristic morphology are presented in Figure S13. The latter data show neurons predominantly localized in the center of cell clusters, and GFAP-expressing glia preferentially located at their exterior, suggesting partial reconstruction of the DRG cellular architecture.

Taken together, these experiments show ability of the RGD-PDL modified surface to present the physicochemical cues sufficient for sustainable cellular network formation followed by development of organotypic (DRG-resembling) structures.

3.4 Topographical Cues of DIW pHH Micropatterns for DRG Cell Outgrowth

To investigate the effects of topographical cues on DRG primary cell outgrowth *in vitro*, we used DIW to fabricate filamentary pHH micropatterns (diameters ranging from 30–100 μm) on a supporting pHH thin-film substrate. After printing and curing (procedures given in the Supplemental Methods), the hydrogel scaffolds were extensively soaked to remove unreacted/otherwise harmful components and then treated with RGD-PDL to confer optimal cell growth properties to the printed structures. Three exemplary micropatterns were selected to compare their distinctive topographical cues. These consisted of a ‘flower’ (that has a spoked geometry), a ‘dendrimer’ (that has a linear branching), and a ‘comb’ (that has periodic anchoring structures along a linear channel). An inspection of the DRG growth and development seen over 14 d in culture showed that the cells respond in pronounced ways to specific attributes of the micropattern geometries. First, the physicochemical cues provided by the different micropatterns induce significant anisotropic outgrowth and more generalized orientation effects (Fig. 3a, 3b **left**, and Fig. S16). Neuronal and glial alignment is accentuated in the immediate proximity of the printed filaments. In the case of the comb array, cells align either within the open linear channels between combs or within the combs in parallel to the nearest adjacent micropatterned features (Supporting Information S16). As

seen in these data, the DRG cells consistently form intricate networks that align with the DIW micropatterned hydrogel features and interconnect with one another via their terminals. These directed cellular microarchitectures survive and develop within the culture over long periods of time (often >4 weeks).

These experiments demonstrate that DRG cells cultured on RGD-PDL-treated pHH micropatterns respond to the physicochemical/mechanical cues presented by the printed features. Surprisingly, even though the micropatterned hydrogel filaments are treated with the same RGD-PDL solution that confers robust growth to their chemically identical (but compositionally distinct) pHH thin film substrates, DRG cells selectively avoid physical attachment to these structures in all cases studied. In point of fact, we found that these structures behave as microwalls that strongly discourage any cellular interconnection or travel across them.

The mechanisms responsible for this surprising behavior are likely complex, and may include the pHH behaving as a reservoir for diffusive chemical depletion of the RGD-PDL from the cell contacting interface by the unmodified pHH present at the filament base as well as to a gradient elastic interface (due to a possible modulus mismatch) present at the filament/substrate edge boundaries,.[78,79] To test the role of depletion effects—wherein diffusion of the activating protein absorbed within the filament into the base substrate lowers its effective available concentration at the cell/gel interface—we added RGD-PDL to the hydrogel ink (RGD-pHH ink) prior to carrying out the DIW patterning (Supplemental Methods). Following scaffold preparation, the RGD-pHH micropatterns and their substrates were then surface-treated with RGD-PDL and subsequently cultured with DRG cells. This modification yields printed RGD-pHH filaments that are fully cell growth compliant. Figure 3b directly compares the distinctive growth and development cues present on scaffolds treated only with RGD-PDL (Fig. 3b, **left**) and scaffolds in which the DIW scaffold was prepared using the RGD-pHH ink (Fig. 3b, **right**). We found here that the subsequent surface treatment with RGD-PDL is essential, as simply supplementing the printable ink with the protein yields poor affinities for cell attachment (Fig. 3b, **middle**). Additional images that show these differences in modes of cell growth are given in Figure S17, and the quantification of these trends is detailed below and presented in Figure 4.

3.5 Quantification of DRG Cell Growth on RGD-pHH Micropatterns

The distinctive cell growth and development regimes that are provided by the printing of a protein-activated pHH hydrogel ink suggest possibilities for the fabrication materials that incorporate biocompatible molecular additives in a grayscale manner to guide and support tissue-mimetic development. Prior to utilizing these materials to construct more complex 3D motifs, we first quantitatively evaluated and compared the relative degree of DRG network development seen on the substrate and the scaffold micropatterns. To do so, the relative surface coverage fractions were determined and statistically evaluated. These data, presented in Figure 4a, confirm that the surface treatment of RGD-pHH microscaffolds with RGD-PDL has the pronounced effect of increasing cell attachment to the filamentous scaffolds, an effect that persists throughout culture times as long as 31 days. The observed effect is robust and active on gel microscaffolds printed on both pHH thin films and more inherently growth

compliant glass substrates (Figure 4a). For example, when pHH scaffolds are printed on either glass or pHH thin films and then subsequently treated with RGD-PDL, robust cell attachment, outgrowth, and cellular network development are seen on the substrate (10–38% surface coverage). Much lower coverage is observed on the scaffold filaments (reaching only 2–7% surface coverage by cellular networks). Cell growth compliance on the DIW scaffold filaments is only conferred by using the RGD-pHH ink and subsequent treatment with RGD-PDL, as confirmed in long term (10 and 20 d) experiments (Fig. 4a). These data show a marked temporal development and reorganization of the DRG cells and their axonal processes on both the supporting substrates and scaffold micropatterns. The incorporation of the RGD-modified PDL into the inks, followed by an RGD-PDL surface treatment, leads to a statistically significant increase in scaffold and cellular coverage— increasing by 100–200% as a result of these modifications when compared to pHH controls. The images presented in Figure 4b show representative confocal fluorescence micrographs of 31 day old cell cultures developed on scaffolds printed with the two ink types, demonstrating that the different modes of cell culture development that the ink modifications engender are both sustainable throughout long culture times and robust.

The data above suggest avenues for realizing programmable forms of DRG cell and organotypic culture development on pHH hydrogel-based microscaffolds by manipulating the diffusion of ECM-mimetic proteins out of the gel mesh of the scaffolds. These findings provide guidance for the architecture of micropatterns that might best facilitate the reconstruction of complex cellular organizations, such as of DRGs and nerves, in culture. In the section that follows, we explore these ideas in studies of DRG cell and organotypic structure development in cultures on 3D micropatterned scaffolds.

3.6 DRG Cellular Networks and Organotypic Structure Development on 3D Scaffolds

To study the morphologies of DRG cell and organotypic structures in cultures developed on 3D RGD-pHH scaffolds, a 9 mm-long channel flanked by inclines of 4 steps, totaling 240 μm in height, was constructed via progressive fusing of 60 μm diameter filaments (Fig. 5a, **schematic**). The geometry of this substrate was chosen so as to favor extensive interactions between cells attached to different steps of the scaffold. The length of the scaffold was selected to allow the observations of the development structural/network features over distances relevant to DRG and nerve repair. Scaffolds adopting this channel geometry were printed using both an unmodified pHH ink, as well as the RGD-pHH ink (Supplemental Methods). Subsequent treatment of the printed scaffolds with RGD-PDL shows the same growth compliance trend observed on the microscaffolds in the previous section, with enhanced cell attachment for scaffolds fabricated using the RGD-pHH ink, as shown and quantified below. The DRG cell cultures developed on the latter scaffolds are viable for extended periods of growth characterized by complex and dynamic morphologies.

A much more pronounced consolidation of cultured DRG cells into ganglion-like constructs on the 3D scaffolds is observed as compared to their 2D counterparts (Fig. 5a, **bottom**, Fig. S19). The DRG cells organize into ganglion-like structures and the cellular terminals consolidate into nerve-resembling bundles interconnecting them. To better characterize this behavior, and the migration patterns that support it within the culture, we carried out an

extensive series of live-cell imaging experiments using spatial light interference microscopy (SLIM). SLIM facilitates label-free long-term imaging and quantitative characterization of live cell dynamics, by combining principles of phase-contrast microscopy and holography to produce interferometric data capable of resolving quantitative features of subcellular dynamics.[80–82] In the current study, we used SLIM to track cell culture consolidation over time in volumes of (17.5 mm) × (17.5 mm) × (0.5 mm) over a period of 128.5 hours, starting at 24 hours after cell seeding. The resulting data showed that the DRG cultures were more dynamic when developed within the open 3D channels, including the consolidation ganglion-like structures over time. Significantly fewer structures were observed after 6 days when compared to day 1. This consolidation is a feature that is less pronounced on 2D scaffolds (Fig. 5b, Fig. S18). The results obtained on the RGD-preloaded scaffold treated with RGD-PDL stand out by their supporting the formation and maintenance of a diversity of cluster sizes over time (Fig. 5c). These scaffolds allow a more dynamic migration of cellular structures, one not observed for the 3D pHH or the 2D scaffolds, with the same surface treatment (Figure S18).

To inquire into the mechanism behind this difference in cell response to the two different ink types on 3D scaffolds, we used the SLIM phase tomograms, which are essentially per-voxel density maps, to provide a quantitative window into the mass transport behavior of the cell culture. To avoid the manual tracking performed in Figure 5b, we turned to *Dispersion-relation phase spectroscopy* which is a fully automatic analysis technique inspired by dynamic light scattering[83,84]. As outlined and applied to tomographic phase volumes in previous work,[85] the analysis scheme automatically characterizes the diffusive and adventive nature of mass transport by looking at the difference through time of the spatial power spectrum. As shown in Tables S5 and S6, the mass transport behavior is comparable between RGD-pHH and pHH open channel 3D scaffolds. We interpret this result to indicate that the differences in cluster size increase over time between the data observed in Figure 5b and those in Figure S18 are not as much due to differences in overall cellular mass transport during the observed time frame, but due to increased initial cell attachment encouraged by the RGD-pHH ink, in agreement with the trends quantified in previous sections.

The latter experiments suggest that control over more complex aspects of organotypic culture development may be possible. These inferences are ones well supported by enhanced activities seen towards consolidation of the 3D DRG cell cultures into ganglion- and nerve-like constructs. Controllable development of organotypic cell cultures creates an opportunity for determination of an improved set of physicochemical design rules for functional devices for cell culture, with potential use in the fields of tissue engineering and regenerative medicine.

4. Conclusion

We describe materials for an engineered 3D cell culture system with cell-growth guiding properties and tunable cell-growth compliance. Chemical modifications of a PDL surface treatment, one traditionally used in cell cultures, have been made to enable access to programmable differences in cell growth behavior on modified pHH films in both a model NIH/3T3 murine fibroblast culture, as well as in the more complex organotypic primary rat

DRG cell culture. We expand on these features in DIW pHH 3D scaffolds to induce cellular network formation on the 3D scaffold filaments by incorporating the RGD-modified PDL into the ink used in the 3D-printing process. The cell-guiding and tissue development capabilities of 3D scaffolds allow for extensive cell network development in 3D. Scaffolds printed with an RGD-pHH ink yield increased formation and consolidation of ganglion-like structures which resemble the native DRG architecture. These scaffolds allow development of tissue-like structures formed from cellular processes, including nerve-like bundles. Understanding what chemistries, topologies, and surface treatments direct growth of neuronal processes in DRG cell cultures is crucial for engineering “smart” scaffolds that can anticipate hierarchical materials requirements for successful functional regeneration of complex nerve tissues. The approach described offers access to a gradient of cell-growth compliance, a tunable degree of scaffold-cell interactions, and control over tissue development in 3D. Our results provide insights to guide future steps that might be taken towards developing dynamic bioactive 3D nerve grafts.

Supplementary Material

Refer to Web version on PubMed Central for supplementary material.

Acknowledgments

The authors would like to thank George A. Ibrahim for helping with cell tracking and SLIM data processing, Lou Ann Miller (Biological Electron Microscopy, Frederick Seitz Materials Research Laboratory, University of Illinois at Urbana-Champaign) for performing the SEM sample preparation, Ryan Pfaff from Keyence for collecting and processing data with the VK-X250 Laser Scanning Microscope, Julio Soares (Laser and Spectroscopy Facility, Frederick Seitz Materials Research Laboratory, University of Illinois at Urbana-Champaign) for assistance and advice regarding confocal fluorescence microscopy, and Professor Prashant Jain’s research group (Chemistry department, University of Illinois at Urbana-Champaign) for use of their UV-Vis spectrometer.

The support of the materials development efforts in the work (J.M.M., R.G.N.) by the U.S. Department of Energy, Division of Materials Sciences under Award # DE-FG02-07ER46471, through the Frederick Seitz Materials Research Laboratory at the University of Illinois at Urbana-Champaign, and of the functional printing methods (A.B., A.W.O., M.B.M.) by the Army Research Office (Award # W911NF-13-0489), are gratefully acknowledged. The support of the National Institute on Drug Abuse through award P30 DA018310 facilitating studies of neuronal cultures (E.G.T., S.S.R., J.V.S.) is also gratefully acknowledged. M.E.K. and G.P. were supported by the National Science Foundation (NSF) Grants CBET-0939511 STC, DBI 14-50962 EAGER, and IIP-1353368.

References

1. Bani-Yaghoub M, Tremblay R, Voicu R, Mealing G, Monette R, Py C, Faid K, Sikorska M. Neurogenesis and Neuronal Communication on Micropatterned Neurochips. Biotechnol Bioeng. 2005; 92:336–345. [PubMed: 16094670]
2. Czöndör K, Garcia M, Argento A, Constals A, Breillat C, Tessier B, Thoumine O. Micropatterned Substrates Coated with Neuronal Adhesion Molecules for High-Content Study of Synapse Formation. Nat Commun. 2013; 4:2252–2265. [PubMed: 23934334]
3. Ravenscroft MS, Bateman KE, Shaffer KM, Schessler HM, Jung DR, Schneider TW, Montgomery CB, Custer TL, Schaffner AE, Liu QY, Li YX, Barker JL, Hickman JJ. Developmental Neurobiology Implications from Fabrication and Analysis of Hippocampal Neuronal Networks on Patterned Silane-Modified Surfaces. J Am Chem Soc. 1998; 120:12169–12177.
4. Vogt AK, Wrobel G, Meyer W, Knoll W, Offenhäusser A. Synaptic Plasticity in Micropatterned Neuronal Networks. Biomaterials. 2005; 26:2549–2557. [PubMed: 15585257]
5. Kleinfeld D, Kahler KH, Hockberger PE. Controlled Outgrowth of Dissociated Neurons on Patterned Substrates. J Neurosci. 1988; 8:4098–4120. [PubMed: 3054009]

6. McCormick AM, Maddipatla MVSN, Shi S, Chamsaz EA, Yokoyama H, Joy A, Leipzig ND. Micropatterned Coumarin Polyester Thin Films Direct Neurite Orientation. ACS Applied Materials & Interfaces. 2014; 6:19655–19667. [PubMed: 25347606]
7. Hardelauf H, Sisnaiske J, Taghipour-Anvari A, Jacob P, Drabiniok E, Marggraf U, Frimat JP, Hengstler JG, Neyer C, van Thriel C, West J. High Fidelity Neuronal Networks Formed by Plasma Masking With a Bilayer Membrane: Analysis of Neurodegenerative and Neuroprotective Processes. Lab Chip. 2011; 11:2763–2771. [PubMed: 21709920]
8. Uz, M., Sharma, AD., Adhikari, P., Sakaguchi, DS., Mallapragada, SK. Development of Multifunctional Films for Peripheral Nerve Regeneration. Acta Biomater. 2016. doi.org/10.1016/j.actbio.2016.09.039
9. Shi P, Scott MA, Ghosh B, Wan DP, Wissner-Gross Z, Mazitschek R, Haggarty SJ, Yanik MF. Synapse Microarray Identification of Small Molecules that Enhance Synaptogenesis. Nat Commun. 2011; 2:510. [PubMed: 22027590]
10. Tuft BW, Xu L, White SP, Seline AE, Erwood AM, Hansen MR, Guymon CA. Neural Pathfinding on Uni- and Multidirectional Photopolymerized Micropatterns. ACS Appl Mater Interfaces. 2014; 6:11265–11276. [PubMed: 24911660]
11. Clarke JC, Tuft BW, Clinger JD, Levine R, Sievens Figueroa L, Guymon CA, Hansen MR. Micropatterned Methacrylate Polymers Direct Spiral Ganglion Neurite and Schwann Cell Growth. Hear Res. 2011; 278:96–105. [PubMed: 21616131]
12. Dertinger SKW, Chiu DT, Jeon NL, Whitesides GM. Generation of Gradients Having Complex Shapes Using Microfluidic Networks. Anal Chem. 2001; 73:1240–1246.
13. Taylor AM, Blurton-Jones M, Rhee SW, Cribbs DH, Cotman CW, Jeon NL. A Microfluidic Culture Platform for CNS Axonal Injury, Regeneration and Transport. Nat Methods. 2005; 2:599–605. [PubMed: 16094385]
14. Romanova EV, Fosser KA, Rubakhin SS, Nuzzo RG, Sweedler JV. Engineering the Morphology and Electrophysiological Parameters of Cultured Neurons by Microfluidic Surface Patterning. FASEB J. 2004; 18:1267–1285. [PubMed: 15208266]
15. Francisco H, Yellen BB, Halverson DS, Friedman G, Gallo G. Regulation of Axon Guidance and Extension by Three-Dimensional Constraints. Biomaterials. 2007; 28:3398–3407. [PubMed: 17467794]
16. Hardelauf H, Waide S, Sisnaiske J, Jacob P, Hausherr V, Schöbel N, Janasek D, van Thriel C, West J. Micropatterning Neuronal Networks. Analyst. 2014; 139:3256–3264. [PubMed: 24855658]
17. Chang JC, Brewer GJ, Wheeler BC. A Modified Microstamping Technique and Enhances Polylysine Transfer Neuronal Cell Patterning. Biomaterials. 2003; 24:2863–2870. [PubMed: 12742724]
18. Jung DR, Kapur R, Adams T, Giuliano KA, Mrksich M, Craighead HG, Taylor DL. Topographical and Physicochemical Modification of Material Surface to Enable Patterning of Living Cells. Crit Rev Biotechnol. 2001; 21:111–154. [PubMed: 11451046]
19. Nagamine K, Hirata T, Okamoto K, Abe Y, Kaji H, Nishizawa M. Portable Micropatterns of Neuronal Cells Supported by Thin Hydrogel Films. ACS Biomaterials Science & Engineering. 2015; 1:329–334.
20. Whitesides GM, Ostuni E, Takayama S, Jiang XY, Ingber DE. Soft Lithography In Biology and Biochemistry. Annu Rev Biomed Eng. 2001; 3:335–373. [PubMed: 11447067]
21. Rogers JA, Nuzzo RG. Recent Progress in Soft Lithography. Materials Today. 2005; 8:50–56.
22. Chen CS, Mrksich M, Huang S, Whitesides GM, Ingber DE. Geometric Control of Cell Life And Death. Science. 1997; 276:1425–1428. [PubMed: 9162012]
23. Bernard A, Renault JP, Michel B, Bosshard HR, Delamarche E. Microcontact Printing of Proteins. Adv Mater. 2000; 12:1067–1070.
24. Offenhaeusser A, Böcker-Meffert S, Decker T, Helpenstein R, Gasteier P, Groll J, Möller M, Reska A, Schäfer S, Schulte P, Vogt-Eisele A. Microcontact Printing of Proteins for Neuronal Cell Guidance. Soft Matter. 2007; 3:290–298.
25. Branch DW, Corey JM, Wehenmeyer JA, Brewer GJ, Wheeler BC. Microstamp Patterns of Biomolecules for High-Resolution Neuronal Networks. Med Biol Eng Comput. 1998; 36:135–141. [PubMed: 9614762]

26. Kane RS, Takayama S, Ostuni E, Ingber DE, Whitesides GM. Patterning Proteins and Cells Using Soft Lithography. Biomaterials. 1999; 20:2363–2376. [PubMed: 10614942]
27. Jeon NL, Choi IS, Kim NY, Harada Y, Finnie KR, Girolami GS, Nuzzo RG, Laibinis PE, Whitesides GM. Patterned Polymer Growth on Silicon Surfaces Using Microcontact Printing and Surface-Initiated Polymerization. Appl Phys Lett. 1999; 75:4201–4203.
28. Frimat JP, Menne H, Michels A, Kittel S, Kettler R, Borgmann S, Franzke J, West J. Plasma Stencilling Methods for Cell Patterning. Anal Bioanal Chem. 2009; 395:601–609. [PubMed: 19449153]
29. Gao Y, Tian J, Wu J, Cao W, Zhou B, Shen R, Wen W. Digital Microfluidic Programmable Stencil (Dmps) for Protein And Cell Patterning. RSC Advances. 2016; 6:101760–101769.
30. Griffith LG, Naughton G. Tissue Engineering—Current Challenges and Expanding Opportunities. Science. 2002; 295:1009–1014. [PubMed: 11834815]
31. Chandran V, Coppola G, Nawabi H, Omura T, Versano R, Huebner EA, Zhang A, Costigan M, Yekkirala A, Barrett L, Blesch A, Michaelevski I, Davis-Turak J, Gao F, Langfelder P, Horvath S, He Z, Benowitz L, Fainzilber M, Tuszynski M, Woolf CJ, Geschwind DH. A Systems-Level Analysis of the Peripheral Nerve Intrinsic Axonal Growth Program. Neuron. 2016; 89:956–970. [PubMed: 26898779]
32. Feirabend, HKP., Marani, E. Dorsal Root Ganglion. In: Aminoff, MJ., Daroff, RB., editors. Encyclopedia of the Neurological Sciences. Academic Press; 2003. p. 28-33.
33. Kandel, ER., Schwartz, JH., Jessell, TM. Principles of Neural Science. 4. McGraw-Hill; New York: 2000. p. 431-433.
34. Scholz J, Woolf CJ. The Neuropathic Pain Triad: Neurons, Immune Cells and Glia. Nat Neurosci. 2007; 10:1361–1368. [PubMed: 17965656]
35. Crain, SM. Physiology of CNS Tissues in Culture. In: Berl, S., editor. Metabolic Compartmentation and Neurotransmission: Relation to Brain Structure and Function. Springer Science & Business Media; 2013. p. 286-7.
36. Adams RD, Rendell SR, Counts LR, Papke JB, Willits RK, Harkins AB. Electrical and Neurotrophin Enhancement of Neurite Outgrowth within a 3D Collagen Scaffold. Ann Biomed Eng. 2014; 42:1282–1291. [PubMed: 24710795]
37. Daud MFB, Pawar KC, Claeyssens F, Ryan AJ, Haycock JW. An Aligned 3D Neuronal-Glial Co-Culture Model for Peripheral Nerve Studies. Biomaterials. 2012; 33:5901–5913. [PubMed: 22656449]
38. Berns EJ, Sur S, Pan L, Goldberger JE, Suresh S, Zhang S, Kessler JA, Stupp SI. Aligned Neurite Outgrowth and Directed Cell Migration in Self-Assembled Monodomain Gels. Biomaterials. 2014; 35:185–195. [PubMed: 24120048]
39. Jha BS, Colello RJ, Bowman JR, Sell SA, Lee KD, Bowlin GL, Chow WN, Mathern BE, Simpson DG, Bigbee JW. Two Pole Air Gap Electrospinning: Fabrication of Highly Aligned Three-Dimensional Scaffolds for Nerve Reconstruction. Acta Biomater. 2011; 7:203–215. [PubMed: 20727992]
40. Liu T, Houle JD, Xu J, Chan BP, Chew SY. Nanofibrous Collagen Nerve Conduits for Spinal Cord Repair. Tissue Eng Part A. 2012; 18:1057–1066. [PubMed: 22220714]
41. Bourke JL, Coleman HA, Pham V, Forsythe JS, Parkington HC. Neuronal Electrophysiological Function and Control of Neurite Outgrowth on Electrospun Polymer Nanofibers Are Cell Type Dependent. Tissue Eng Part A. 2014; 20:1089–1095. [PubMed: 24147808]
42. Xie J, MacEwan MR, Liu W, Jesuraj N, Li X, Hunter D, Xia Y. Nerve Guidance Conduits Based on Double-Layered Scaffolds of Electrospun Nanofibers for Repairing the Peripheral Nervous System. ACS Appl Mater Interfaces. 2014; 6:9472–9480. [PubMed: 24806389]
43. Johnson BN, Lancaster KZ, Zhen G, He J, Gupta MK, Kong YL, Engel EA, Krick KD, Ju A, Meng F, Enquist LW, Jia X, McAlpine MC. 3D Printed Anatomical Nerve Regeneration Pathways. Adv Funct Mater. 2015; 25:6205–6217. [PubMed: 26924958]
44. Klebe RJ. Cytoscribing: a Method for Micropositioning Cells and the Construction of Two- and Three-Dimensional Synthetic Tissues. Exp Cell Res. 1988; 179:362–373. [PubMed: 3191947]

45. Xu T, Zhao W, Zhu JM, Albanna MZ, Yoo JJ, Atala A. Complex Heterogeneous Tissue Constructs Containing Multiple Cell Types Prepared by Inkjet Printing Technology. Biomaterials. 2013; 34:130–139. [PubMed: 23063369]
46. Xu T, Jin J, Gregory C, Hickman JJ, Boland T. Inkjet Printing of Viable Mammalian Cells. Biomaterials. 2005; 26:93–99. [PubMed: 15193884]
47. Cui X, Boland T, D'Lima DD, Lotz MK. Thermal Inkjet Printing in Tissue Engineering and Regenerative Medicine. Recent Pat Drug Deliv Formul. 2012; 6:149–155. [PubMed: 22436025]
48. Cohen DL, Malone E, Lipson H, Bonassar LJ. Direct Freeform Fabrication of Seeded Hydrogels in Arbitrary Geometries. Tissue Eng. 2006; 12:1325–1335. [PubMed: 16771645]
49. Iwami K, Noda T, Ishida K, Morishima K, Nakamura M, Umeda N. Bio Rapid Prototyping by Extruding/Aspirating/Refilling Thermoreversible Hydrogel. Biofabrication. 2010; 2:014108.doi: 10.1088/1758-5082/2/1/014108 [PubMed: 20811123]
50. Shor L, Güçeri S, Chang R, Gordon J, Kang Q, Hartsock L, An Y, Sun W. Precision Extruding Deposition (PED) Fabrication of Polycaprolactone (PCL) Scaffolds for Bone Tissue Engineering. Biofabrication. 2009; 1:015003.doi: 10.1088/1758-5082/1/1/015003 [PubMed: 20811098]
51. Barron JA, Wu P, Ladouceur HD, Ringeisen BR. Biological Laser Printing: a Novel Technique for Creating Heterogeneous 3-Dimensional Cell Patterns. Biomed Microdevices. 2004; 6:139–147. [PubMed: 15320636]
52. Guillemot F, Souquet A, Catros S, Guillotin B, Lopez J, Faucon M, Pippenger B, Bareille R, Rémy M, Bellance S, Chabassier P, Fricain JC, Amédée J. High- Throughput Laser Printing of Cells and Biomaterials For Tissue Engineering. Acta Biomater. 2010; 6:2494–2500. [PubMed: 19819356]
53. Guillotin B, Souquet A, Catros S, Duocastella M, Pippenger B, Bellance S, Bareille R, Rémy M, Bordenave L, Amédée J, Guillemot F. Laser Assisted Bioprinting of Engineered Tissue with High Cell Density and Microscale Organization. Biomaterials. 2010; 31:7250–7256. [PubMed: 20580082]
54. Sun L, Parker ST, Syoji D, Wang X, Lewis JA, Kaplan DL. Direct-Write Assembly of 3D Silk/Hydroxyapatite Scaffolds for Bone Co-Cultures. Adv Healthc Mater. 2012; 1:729–735. [PubMed: 23184824]
55. Peltola SM, Melchels FP, Grijpma DW, Kellomaki M. A Review of Rapid Prototyping Techniques for Tissue Engineering Purposes. Ann Med. 2008; 40:268–280. [PubMed: 18428020]
56. Hansen CJ, Saksena R, Kolesky DB, Vericella JJ, Kranz SJ, Muldowney GP, Christensen KT, Lewis JA. High-Throughput Printing Via Microvascular Multinozzle Arrays. Adv Mater. 2013; 25:96–102. [PubMed: 23109104]
57. Drury JL, Mooney DJ. Hydrogels for Tissue Engineering: Scaffold Design Variables and Applications. Biomaterials. 2003; 2:4337–4351.
58. Murphy SV, Atala A. 3D Bioprinting of Tissues and Organs. Nat Biotechnol. 2014; 32:773–785. [PubMed: 25093879]
59. Gladman AS, Matsumoto EA, Nuzzo RG, Mahadevan L, Lewis JA. Biomimetic 4D Printing. Nat Materials. 2016; 15:413–419. [PubMed: 26808461]
60. Kirschner CM, Anseth KS. Hydrogels In Healthcare: From Static to Dynamic Material Microenvironments. Acta Materialia. 2013; 61:931–944. [PubMed: 23929381]
61. Indolfi L, Causa F, Netti PA. Coating Process and Early Stage Adhesion Evaluation of Poly(2-Hydroxy-Ethyl-Methacrylate) Hydrogel Coating of 316L Steel Surface for Stent Applications. Journal Of Materials Science: Materials In Medicine. 2009; 20:1541–1551. [PubMed: 19267260]
62. Wichterle O, Lim D. Hydrophilic Gels for Biological Use. Nature. 1960; 185:117–118.
63. Montheard JP, Chatzopoulos M, Chappard D. 2-Hydroxyethylmethacrylate (HEMA): Chemical Properties and Applications in Biomedical Fields. JMS-Rev Macromol Chem Phys. 1992; C32:1–34.
64. McCracken JM, Badea A, Kandel ME, Gladman AS, Wetzel DJ, Popescu G, Lewis JA, Nuzzo RG. Programming Mechanical and Physicochemical Properties of 3D Hydrogel Cellular Microcultures Via Direct Ink Writing. Adv Healthc Mater. 2016; doi: 10.1002/Adhm.201500888
65. Hanson Shepherd JN, Parker ST, Shepherd RF, Gillette MU, Lewis JA, Nuzzo RG. 3D Microperiodic Hydrogel Scaffolds for Robust Neuronal Cultures. Adv Funct Mater. 2011; 21:47–54. [PubMed: 21709750]

66. Ruoslahti E, Pierschbacher MD. New Perspectives in Cell Adhesion: RGD and Integrins. Science. 1987; 238:491–497. [PubMed: 2821619]

67. Hynes RO. Integrins: Bidirectional, Allosteric Signaling Machines. Cell. 2002; 110:673–687. [PubMed: 12297042]

68. Popescu, G. Quantitative Phase Imaging of Cells And Tissues. Mcgraw-Hill; 2011.

69. Wang Z, Millet L, Mir M, Ding H, Unarunotai S, Rogers JA, Gillette MU, Popescu G. Spatial Light Interference Microscopy (SLIM). Opt Express. 2011; 19:1016. [PubMed: 21263640]

70. Jacobson BS, Branton D. Plasma Membrane: Rapid Isolation and Exposure of the Cytoplasmic Surface by Use of Positively Charged Beads. Science. 1977; 195:302–304. [PubMed: 831278]

71. Nevo A, De Vries A, Katchalsky A. Interaction of Basic Polyamino Acids with the Red Blood Cell I. Combination of Polylysine with Single Cells. Biochimica Et Biophysica Acta. 1955; 17:536–547. [PubMed: 13250001]

72. Carlsson J, Drevin H, Axen R. Protein Thiolation and Reversible Protein-Protein Conjugation. Biochem J. 1978; 173:723–737. [PubMed: 708370]

73. Ardjoandi N, Klein C, Kohler K, Maurer A, Kalbacher H, Niederländer J, Reinert S, Alexander D. Indirect Coating of RGD Peptides Using a Poly-L-Lysine Spacer Enhances Jaw Periosteal Cell Adhesion, Proliferation and Differentiation into Osteogenic Tissue. J Biomed Mater Res Part A. 2012; 100A:2034–2044.

74. Grotzky A, Manaka Y, Fornera S, Willeke M, Walde P. Quantification of α-Polylysine: a Comparison of Four UV/Vis Spectrophotometric Methods. Anal Methods. 2010; 2:1448–1455.

75. Liu R, Lin G, Xu H. An Efficient Method for Dorsal Root Ganglia Neurons Purification with a One-Time Anti-Mitotic Reagent Treatment. PLOS One. 2013; 8:E60558. [PubMed: 23565257]

76. Leifer D, Lipton SA, Barnstable CJ, Masland RH. Monoclonal Antibody to Thy-1 Enhances Regeneration of Processes by Rat Retinal Ganglion Cells in Culture. Science. 1984; 224:303–306. [PubMed: 6143400]

77. Öztürk G, Erdoğan E. Multidimensional Long-Term Time-Lapse Microscopy of in Vitro Peripheral Nerve Regeneration. Microscopy Research And Technique. 2004; 64:228–242. [PubMed: 15452890]

78. Huang WC, Liu KH, Liu TC, Liu DM, Chen SY. Synergistic Hierarchical Silicone-Modified Polysaccharide Hybrid as a Soft Scaffold to Control Cell Adhesion and Proliferation. Acta Biomaterialia. 2014; 10:3546–3556. [PubMed: 24793655]

79. Raja WK, Gligorijevic B, Wyckoff J, Condeelis JS, Castracane J. A New Chemotaxis Device for Cell Migration Studies. Integrative Biology. 2010; 2:696–706. [PubMed: 20938544]

80. Wang Z, Millet L, Chan V, Ding H, Gillete MU, Bashir R, Popescu G. Label-Free Intracellular Transport Measured by Spatial Light Interference Microscopy. J Biomed Opt. 2011; 16:026019. [PubMed: 21361703]

81. Kandel ME, Teng KW, Selvin PR, Popescu G. Label-Free Imaging of Single Microtubule Dynamics Using Spatial Light Interference Microscopy. ACS Nano. 2017; 11:647–655. [PubMed: 27997798]

82. Mir M, Kim T, Majumder A, Xiang M, Wang R, Liu SC, Gillette MU, Stice S, Popescu G. Label-Free Characterization of Emerging Human Neuronal Networks. Sci Rep. 2014; 4:4434. [PubMed: 24658536]

83. Wang R, Wang Z, Millet L, Gillette MU, Levine AJ, Popescu G. Dispersion-Relation Phase Spectroscopy of Intracellular Transport. Opt Express. 2011; 19:20571. [PubMed: 21997064]

84. Brown, W., editor. Dynamic Light Scattering: The Method and Some Applications. 1. Oxford University Press; 1993. (Monographs on the Physics and Chemistry of Materials)

85. Kandel ME, Fernandes D, Taylor AM, Shakir H, Best-Popescu C, Popescu G. Three-Dimensional Intracellular Transport in Neuron Bodies And Neurites Investigated by Label-Free Dispersion-Relation Phase Spectroscopy. Cytometry Part A. 2017; doi: 10.1002/Cyto.A.23081

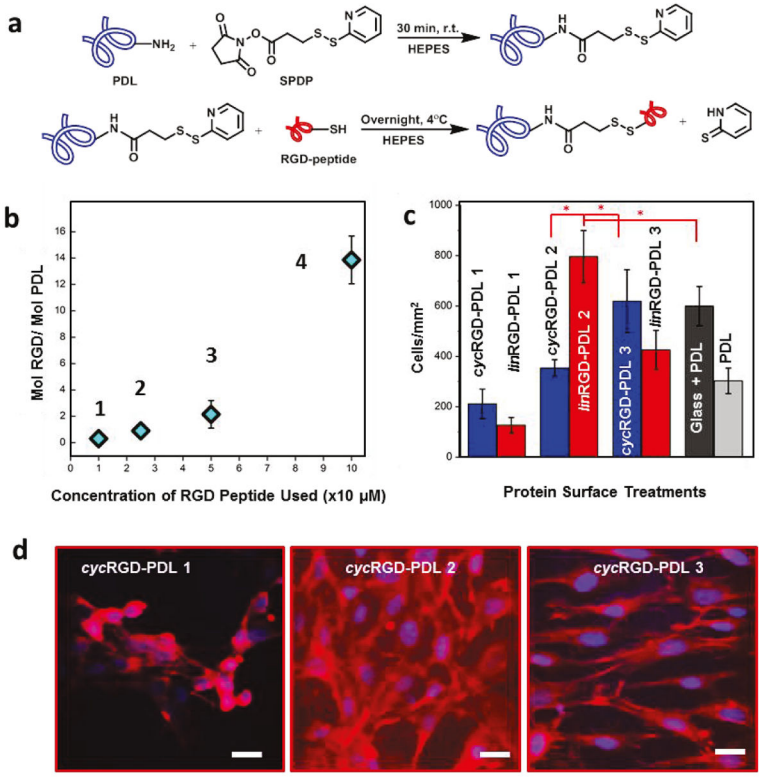

Figure 1. Modified PDL Synthesis and Assessment of RGD-dependence of Cell Growth and Morphology using NIH/3T3 Embryonic Murine Fibroblasts

(a) Covalent coupling mechanism between PDL and RGD-containing peptides. **(b)** Plot illustrating *cyc*(*lin*)RGD-PDL 1–4 as the degree of the RGD modification of PDL. Error bars represent standard deviations and are smaller than data point diamonds for 1 and 2. **(c)** NIH/3T3 fibroblast cell densities at 24 hours in culture on different surface treatments. Tukey's means comparisons (Supplementary Information, Table S1) are highlighted by red asterisks, $p < 0.01$. **(d)** CFM Images of 3T3 fibroblasts on representative surface treatments 24 hours after seeding. Actin filaments stained with rhodamine-phalloidin (red), and nuclei stained withDAPI (blue). Scale bar is 15 μm.

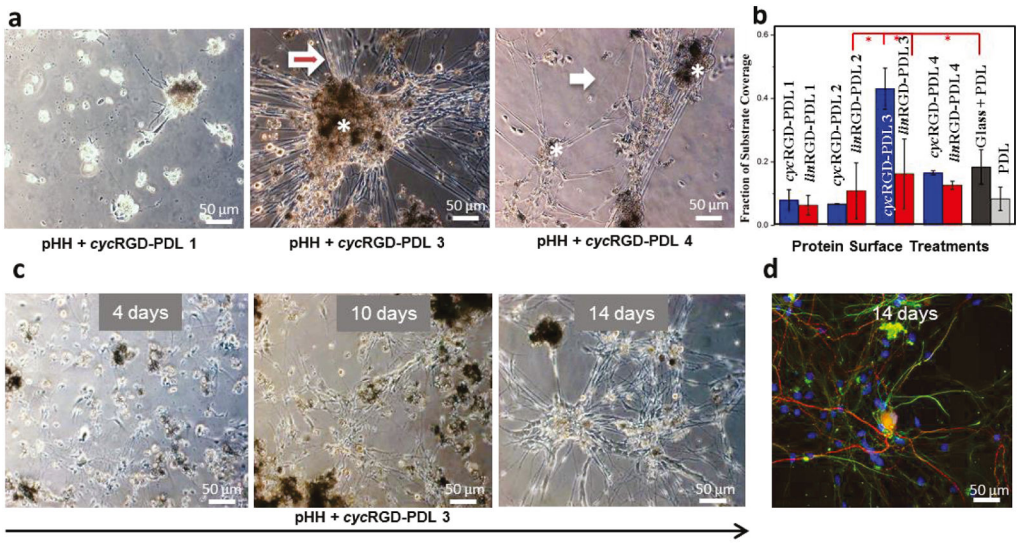

Figure 2. Attributes of RGD-Modified PDL Surface Treatment Showing DRG Cell Culture Optimal Temporal Progression and Glia-Neurons Association

(a) Phase contrast inverted microscope images of DRG cells on different surface treatments after ~9 days in culture. Cell bodies range orange-dark brown. White asterisks mark cell clusters. The white arrows point to individual cell terminals, while the red asterisks mark bundles of terminals, more frequently extending out of cell clusters. **(b)** Surface area coverage of DRG cells as a response to *cyc* (blue bars) and *lin* (red bars) RGD-PDL surface treatments after ~9 days in culture. Tukey's mean comparisons are presented in Supplementary Information, Table S2. Key differences are highlighted by red asterisks, $p < 0.0001$. **(c**) DRG cell culture development over time on pHEMA spin-coated glass slides treated with cycRGD-PDL 3. **(d)** Confocal fluorescence micrograph of (c) showing the different types of cells: neurons (red) and glia (green). Cell nuclei are blue.

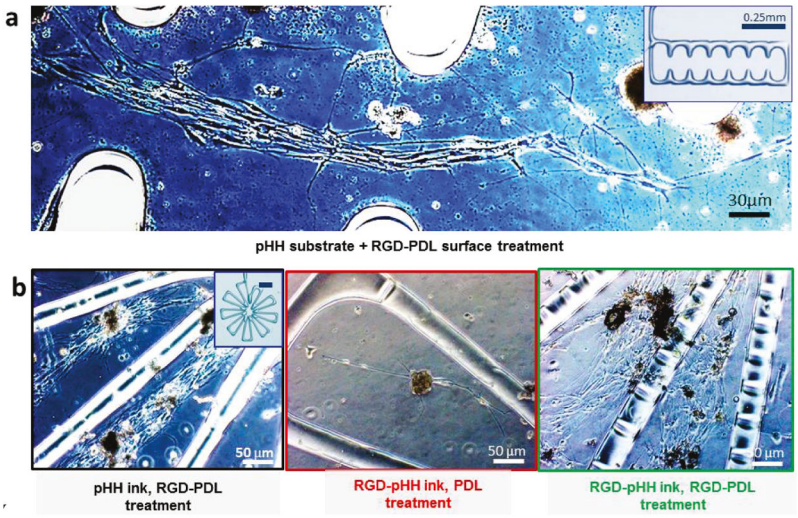

Figure 3. DRG Cell Culture on 3D Direct-Write Assembled Structures Demonstrates Impact on Growth of Aspect Ratios and Diffusible Molecules

(a) DRG cell response to guidance cues of pHEMA 3D-printed scaffolds of various geometries. Filament diameter: 50µm. **(b)** Increased DRG cell attachment and process development on RGD-pHH filaments with RGD-PDL (right) vs. PDL treatment (center). Increased cell networking on the filaments (right) vs. mainly in the interfilamentous space (left) is observed.

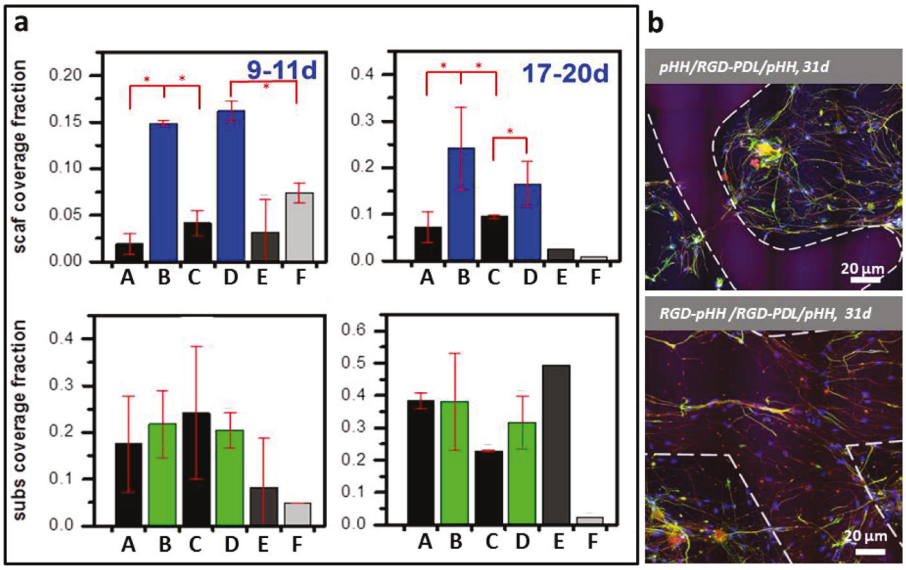

Figure 4. Quantitative Comparison of DRG Cell Surface Area Coverage as a Function of Ink Chemistry and Surface Treatment

(a) Surface area coverage measured for primary DRG cells on their scaffolds and substrates at short (9–11d) and long (17–20d) culture times. Conditions are described as scaffold material/surface treatment/substrate: A - RGD-pHH/PDL/glass, B - RGD-pHH/RGD-PDL/glass, C- RGD-pHH/PDL/pHH, D- RGD-pHH/RGD-PDL/pHH, E - pHH/RGD-PDL/glass, F - pHH/RGD-PDL/pHH. The data points represent results from each set of conditions tested on 5–12 scaffolds. Error bars represent standard deviations. KeyTukey's means comparisons (Tables S3 and S4) are highlighted by red asterisks, $p < 0.0001$. **(b)** Confocal fluorescence micrographs showing long lasting effects of RGD-ink scaffolds in increasing cell networking on scaffold filaments. The white lines represent the outline of the scaffold filaments. Immunocytochemistry: nuclei (blue), neurons (red) and glia (green).

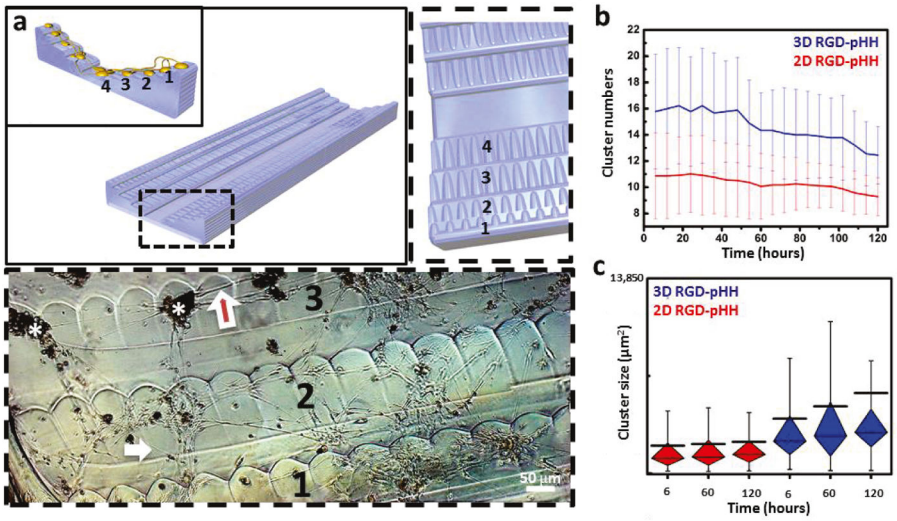

Figure 5. Controlling the degree of consolidation of DRG cell networks with 3D Scaffolds

(a) Schematic of the 3D scaffold geometry: channel flanked by staircases to allow for 3D connections between DRG cells attached to different levels (1–4, inset schematic). Dashed box (top left schematic) shows an expanded view of step structural details. Dashed box (bottom) shows a phase contrast inverted micrograph of DRG cells on the scaffold treated with RGD-PDL at ~9 days in culture. Cell bodies range orange-dark brown. White asterisks mark cell clusters. The white arrows point to individual cell terminals, while the red arrows mark bundles of terminals, more frequently extending out of cell clusters. **(b)** Consolidation of clusters over time on RGD-pHH scaffolds in 2D (red) and 3D (blue). The 3D scaffold leads to a significant decrease in cell cluster numbers over time. Error bars represent standard deviation. **(c)** Box and whiskers plots showing the increase in cluster size over time facilitated by the 3D scaffolds (blue) but not the 2D scaffolds (red). The black line represents the mean, showing the increase of overall size of clusters over time in 3D. Whiskers extend to the minima and maxima of 90% of the data. Box is divided by the median line into first quartile (bottom part) and third quartile (top part) of the data.

Table 1

NIH/3T3 Growth/Attachment and Morphology on RGD-PDL-coated pHH films

RGD-PDL protein quantification				**spatial morphological properties**			
composition		**population *(cells/mm^2)***		**Distribution**		**Density**	
type	***ratio***	***cyc*RGD-PDL**	***lin*RGD-PDL**	***cyc*RGD-PDL**	***lin*RGD-PDL**	***cyc*RGD-PDL**	***lin*RGD-PDL**
1	0.3:1	212 ± 59	127 ± 31	cluster	cluster	Low	low
2	0.9:1	353 ± 33	796 ± 103	uniform	uniform	Med	high
3	2.1:1	619 ± 125	426 ± 77	uniform	uniform	High	med
4	13.9:1	--	--	cluster	cluster	Low	low
0	0:1	303 ± 50		Cluster		Low	
G	0:1	599± 78		Uniform		High	

G—glass; type 0 – PDL; ratio – RGD-containing peptide: PDL

Table 2

DRG Surface Coverage on RGD-PDL-coated pHH films

RGD-PDL composition		**surface coverage (*day 9*)**	
type	***ratio***	***cyc*RGD-PDL**	***lin*RGD-PDL**
1	0.3:1	**0.08 ± 0.03**	0.06 ± 0.03
2	0.9:1	**0.07 ± 0.001**	0.11 ± 0.09
3	2.1:1	**0.43 ± 0.06**	0.16 ± 0.11
4	13.9:1	**0.17 ± 0.07**	0.13 ± 0.01
0	0:1	0.08 ± 0.04	
G	0:1	0.18 ± 0.05	

G— glass; type 0 – PDL; ratio – RGD-containing peptide: PDL; surface coverage – fraction of sample surface occupied by DRG cells